Combined Numerical and Experimental Investigation of Localized Electroporation-Based Cell Transfection and Sampling

Prithvijit Mukherjee[1, 2, *], S. Shiva P. Nathamgari[1, 2, *], John A. Kessler[3], Horacio D. Espinosa[1, 2, 4]

[1]Department of Mechanical Engineering, Northwestern University, Evanston IL-60208, United States

[2]Theoretical and Applied Mechanics Program, Northwestern University, Evanston IL-60208, United States

[3]Department of Neurology, Northwestern University, Chicago, IL-60611, United States

[4]Corresponding author: espinosa@u.northwestern.edu, [*]equal contribution

Supporting Information Table 1: Parameters used in Lumped Circuit Model

W	$R_g/(R_g + R_{cy})$
X	$WR_{cy} + R_{cp} + R_{op}$
Y	$R_s + R_{op}\left(1 - R_{op}/X\right)$
Z	$1 - R_{cy}/(R_g + R_{cy})$
n_1	$1/(YC_c)$
n_2	$-1/C_c\left(1/R_c + 1/Y\right)$
n_3	$-WR_{op}/(XYC_c)$
n_4	$ZR_{op}/(XYC_t)$
n_5	$-1/C_t\left(1/R_t + ZR_{op}^2W/X^2Y + WZ/X + 1/(R_g + R_{cy})\right)$
n_6	$-1/C_t\left(ZR_{op}^2W/X^2Y + WZ/X + 1/(R_g + R_{cy})\right)$
n_7	$ZR_{op}/(XYC_b)$

n_8	$-1/C_b\left(ZR_{op}^2W/X^2Y + WZ/X + 1/(R_g + R_{cy})\right)$
n_9	$-1/C_b\left(1/R_b + ZR_{op}^2W/X^2Y + WZ/X + 1/(R_g + R_{cy})\right)$

Supporting Information S1: Coupling between Electric Field and Pore Evolution Equations

The formation of electro-pores leads to a change in the conductivity of the cell membrane. This is incorporated in the model by modifying the cell membrane resistances R_t and R_b at every time step based on the distribution of electropores obtained from the Smoluchowski equation. The total cell membrane resistance is given by –

$$1/R = 1/R_m + \sum 1/R_p \quad (1)$$

Here, R is the total membrane resistance $\left(d_m/\kappa A\right)$ where d_m is the thickness of the cell membrane, κ is the effective cell membrane conductivity and A is the total area of the cell membrane. In our case R is R_t or R_b. R_m is the resistance of the cell membrane and R_p is the resistance of one electro-pore. The summation is over all the electro-pores present at a particular time.

We have, $R_m = R_m'/(1 - A_f)$; where R_m' is the resistance of the intact cell membrane without electro-pores and A_f is the area fraction of the membrane covered by electro-pores present at a particular time step. For our model $R_m' = d_m/\kappa' A$ and $A_f = \int_{r_{min}}^{r_{max}} n\pi r_p^2 dr_p$ where κ' is the conductivity of the intact cell membrane. The overall resistance of an electro-pore is given by $R_p = d_m/2\kappa_p A_p H_p K_p + 1/2\kappa_p r_p$ where κ_p is the pore conductivity, A_p is the area of the pore and H_p and K_p are the hindrance and partition factors respectively.[1]

Supporting Information S2: Hydrophilic Pore Energy and Tension Coupled Pores

The energy difference (E) between an intact lipid bilayer membrane and one with a hydrophilic electro-pore as a function of the radius of the pore (r_p) is given by –

$$E(r_p) = \beta\left(\frac{r_{min}}{r_p}\right)^4 + 2\pi\gamma r_p - \sigma_e \pi r_p^2 - \int_{r_{min}}^{r_p} F(r', V_m)dr' \quad (2)$$

The first term arises due to the steric repulsion between lipid heads with β representing the steric repulsion energy.[2] The second term is due to the line tension along the pore perimeter where γ is the edge energy.[3] The third term accounts for the reduction of membrane tension and consequently the membrane energy due to the formed pore with σ_e being the effective membrane tension.[4] The final term which takes the form of work done by an electric field on a dielectric body is the contribution of the TMP (V_m) in reducing the energy.[5] The non-linear form of the effective membrane tension (σ_e) which couples the electro-pores is given by-[4]

$$\sigma_e = 2\sigma' - \frac{2\sigma' - \sigma}{\left(1 - A_f\right)^2} \quad (3)$$

Here, σ' is the energy of the hydrocarbon-water interface, σ is the surface tension of the membrane without pores and A_f is the area fraction of pores as discussed before. The function $F(r, V_m)$, which represents the electric force is given by-[5]

$$F(r, V_m) = \frac{F_{max}}{1 + {r_h}/{(r + r_t)}} V_m^2 \quad (4)$$

Where, F_{max}, r_h and r_t are constants.

Supporting Information S3: Pore Creation and Destruction Rates

The Smoluchowski equation is solved in the pore radius space to obtain the pore distribution at every time step. At the minimum radius (r_m) an Arrhenius-type expression is used as the boundary condition to account for the nucleation and destruction of electro-pores-[6]

$$-\left(D_p\frac{\partial n}{\partial r_p}+\frac{D_p}{kT}n\frac{\partial E}{\partial r_p}\right)=Ae^{\frac{BV_m^2}{kT}}-\nu n \tag{5}$$

Here, A is the pore creation rate density, B is the pore creation constant and ν is the pore destruction constant derived by assuming an absorption condition slightly below r_{min}.[1]

At the maximum radius (r_{max}), a no flux boundary condition is used-

$$D_p\frac{\partial n}{\partial r_p}+\frac{D_p}{kT}n\frac{\partial E}{\partial r_p}=0 \tag{6}$$

Supporting Information S4: Hindrance and Partition

Due to the finite size and charge of a molecule, their transport through a pore in a dielectric media is impeded as compared to the bulk electrolyte. The hindrance and partition factors are introduced to account for the impeded transport.

A spherical molecule of finite size is obstructed due to the decreased effective area of pore available for transport and drag from the pore walls.[7,8] The hindrance factor H_p is a continuum approximation that accounts for these effects –

$$H_p=f_Af_D \tag{7}$$

Here, f_A is the area factor and f_D drag factor. The area factor f_A is given by –

$$f_A = \left(1 - \frac{r_s}{r_p}\right)^2 \tag{8}$$

Where, r_s is the radius of the molecule and r_p is the radius of the pore.

The drag factor f_D is given by –

$$f_D = \frac{6\pi}{f_t} \tag{9}$$

Where f_t is –

$$f_t = \frac{9}{4}\pi^2\sqrt{2}(1-\lambda)^{-\frac{5}{2}}(1 + a_1(1-\lambda) + a_2(1-\lambda)^2) + a_3 + a_4\lambda + a_5\lambda^2 + a_6\lambda^3 + a_7\lambda^4 \tag{10}$$

Here, $\lambda = r_s/r_p$. The constants a_1 to a_7 are provided in Supporting Information Table 3.

The partition factor accounts for the non-ohmic behavior of a pore formed in a membrane that affects the transport of charged specie across it. The electrostatic interaction of a charged molecule with the pore wall leads to higher energy of the molecule inside the dielectric membrane pore as compared to the bulk electrolyte, as shown by Parsegian.[9] Thus, there is an energy barrier hindering the transport of charged molecules into the membrane pores, which increases with decreasing pore size. Assuming a trapezoidal energy profile inside a membrane pore, Chernomordik et al.[10] developed an equation for the partition function K_p –

$$K_p = \frac{e^{\Delta\psi_m} - 1}{\frac{w_0 e^{w_0 - n_r\Delta\psi_m} - n_r\Delta\psi_m}{w_0 - n_r\Delta\psi_m} e^{\Delta\psi_m} - \frac{w_0 e^{w_0 + n_r\Delta\psi_m} + n_r\Delta\psi_m}{w_0 + n_r\Delta\psi_m}} \tag{11}$$

Here, n_r is the relative entrance length of the pore and $\Delta\psi_m$ is the dimensionless transmembrane potential –

$$\Delta\psi_m = \frac{ez}{kT}V_m \tag{12}$$

Where, e is the electronic charge, z is the valency of the molecule of interest and V_m is the transmembrane potential.

In equation 7, w_0 is the Born Energy,[6, 9] which in this context is the energy required to place a unit charge from the bulk medium into the dielectric membrane pore –

$$w_0 = 5.3643\frac{(ez)^2}{kT}r_p^{-1.803} \quad (13)$$

Supporting Information S5: Verification of Multiphysics Model

The Boltzmann distribution satisfies the steady state Smoluchowski equation.[11] In order to verify the model, the normalized pore distribution ($n/\sum n$) at steady state, obtained from the numerical simulation, was compared to the analytical Boltzmann distribution ($e^{-E/kT}/\sum e^{-E/kT}$) where, E is the hydrophilic pore energy calculated using equation 2. We found close agreement of the two solutions (**see Supporting Information Figure 6**). The pore distribution (n) obtained from the numerical simulation was also plotted for different mesh sizes and the solutions were found to converge (**see Supporting Information Figure 6**). The mesh element size was fixed at 0.05 nm, which ensured that the Peclet Number is <1 and no numerical instability is encountered while solving the Smoluchowski equation.

Supporting Information Table 2: Parameters used in Pore Evolution Equation

Parameters for the model are obtained from relevant literature.[1, 4] The important parameters used in the model are listed below -

PARAMETER	VALUE
κ' , Membrane conductivity	5×10^{-7} S/m
κ_p , Pore conductivity	1 S/m
d_m , cell membrane thickness	5 nm
r_{min} , Minimum electro-pore radius	0.65 nm
r_{max} , Maximum electro-pore radius	15 nm
β , Steric repulsion energy	1.4×10^{-19} J
γ , Edge energy	2×10^{-11} J m^{-1}
σ , Initial membrane tension	Varied over a range (see main text)
σ' , Hydrocarbon-water interface tension	20×10^{-3} J m^{-2}
F_{max} , Maximum electric force	6.9×10^{-10} N/V^2
r_h , Electric force constant	0.95 nm
r_t , Electric force constant	0.23 nm
D_p , Pore diffusion coefficient	2×10^{-13} m^{2}s^{-1}
A , Pore creation rate density	1×10^{9} m^{-2}s^{-1}
B , Pore creation constant	20 kT/V^2
T , Temperature	310 K
D , Diffusion coefficient of molecule	3×10^{-11} m^{2}s^{-1}

Supporting Information Table 3: Parameters used in Transport Equation

PARAMETER	VALUE
r_s, Radius of molecule	3 nm
a_1	-1.2167
a_2	1.5336
a_3	-22.5083
a_4	-5.6117
a_5	-0.3363
a_6	-1.2160
a_7	1.6470
n_r, Relative entrance length	0.25

Supporting Information Figure 1: Nanochannel density and cell confluency affect electroporation efficiency

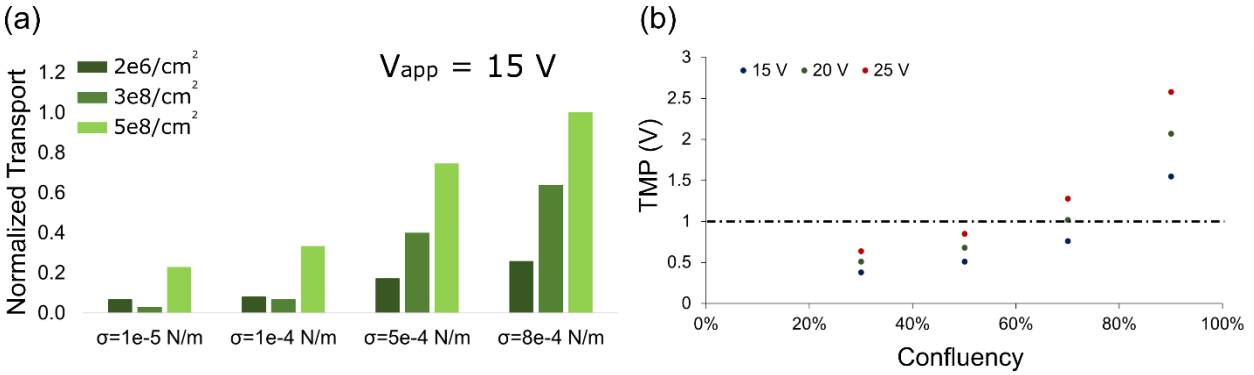

Supporting Information Figure 1: Effect of nanochannel density and cell confluency (a) The normalized transport is plotted for polycarbonate substrates with different nanochannel densities for varying membrane tensions. The transport is found to increase with increasing nanochannel density. The applied voltage is 15 V, (b) The TMP obtained from the equivalent circuit model without pore evolution is plotted as a function of cell confluency for different applied voltages. It is found that the confluency should be above ~80% for the TMP to exceed the critical value of 1 V. The nanochannel density used in these calculations is 5e8/cm^2.

Supporting Information Figure 2: Transport of small molecules (PI) is insensitive to the membrane tension

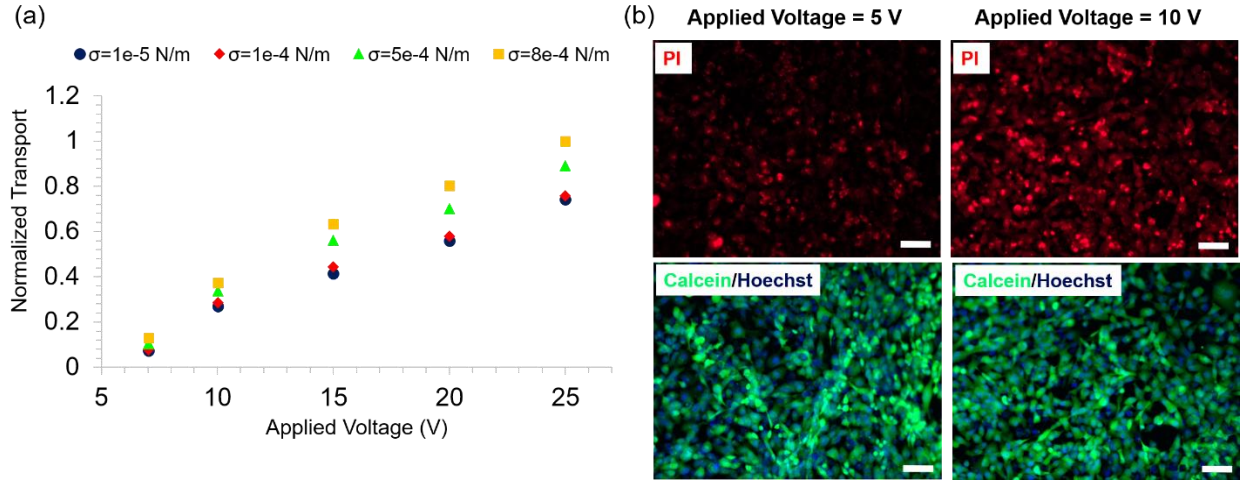

Supporting Information Figure 2: Transport of Small Molecules (a) The normalized transport obtained from the simulations is plotted against the applied far-field voltage (V_{app}) for different values of membrane tension (σ). The transport of small molecules increases linearly with V_{app} and shows lower sensitivity with increasing σ as compared to that of large molecules, (b) PI is delivered into HT 1080 cells under iso-osmolar conditions. Top fluorescence images show the delivery of PI at two different applied voltages (5 V and 10 V). The fluorescence intensity is enhanced with an increase in V_{app} from 5 V to 10 V indicating increased transport. Bottom fluorescence images indicate the corresponding cell viability (>95%) after 6 hours using live dead staining.

Supporting Information Figure 3: Transfection of mCherry plasmid in HT 1080 cells under different voltage amplitudes

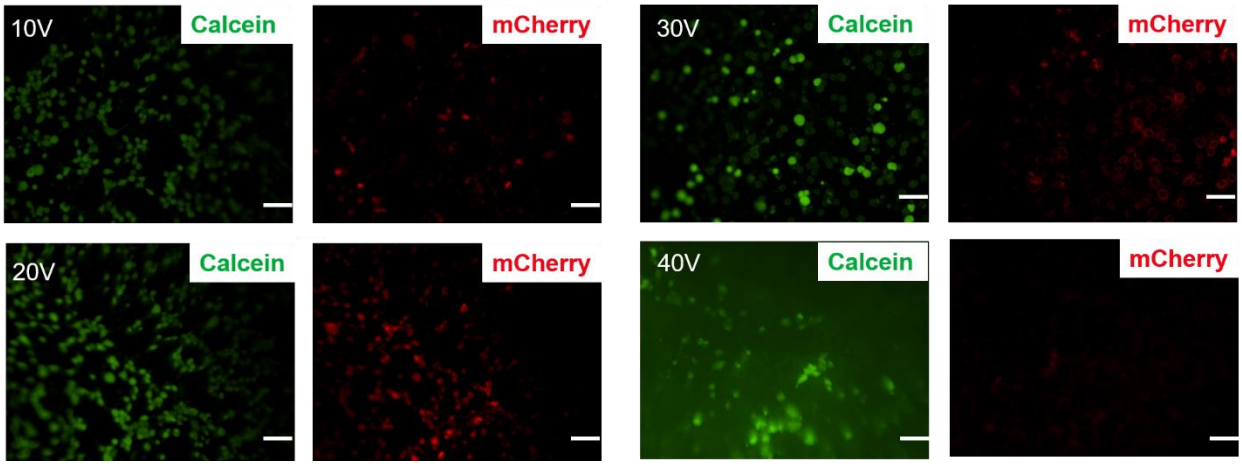

Supporting Information Figure 3: The transfection efficiency of mCherry plasmid (1 day after electroporation) and cell-viability in HT 1080 cells were investigated under various voltage amplitudes. The cell-viability and transfection efficiency were optimal for 30 V. Scale bars = 50 µm in all images.

Supporting Information Figure 4: Small pores remain open even after the electroporation pulse as predicted by the model and inferred from the quenching of Calcein AM in CHO cells

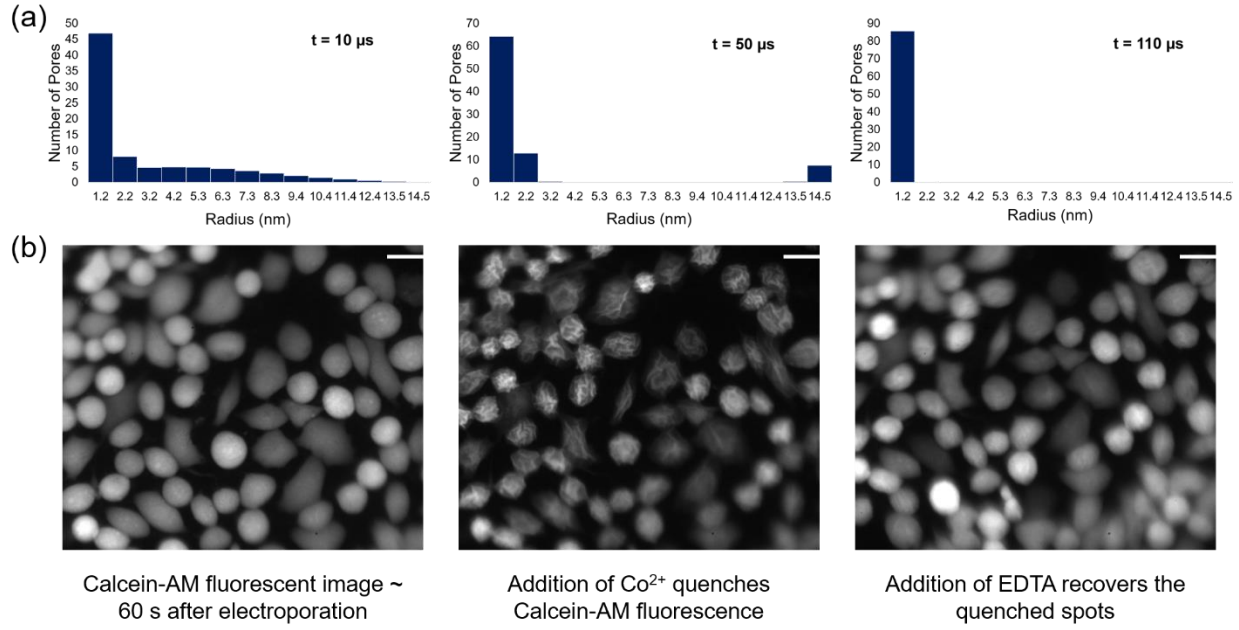

Supporting Information Figure 4: Existence of small pores post pulsation (a) Histogram of pore sizes for a 10 V pulse of 100 µs duration at 1e-5 N/m membrane tension. Large pore (> 3 nm) populations exist during the pulse (Left and Middle). Only a population of small pores (<1.5 nm) remain after the pulse (Right), (b) Co^{2+} is introduced into electroporated CHO cells approximately 1 minute after the pulse ends. The addition of Co^{2+} results in a quenching of the green fluorescence signal, which is later recovered (~3 mins) by introducing a chelating buffer (EDTA). The quenching and subsequent recovery indicate that small pores remain open even after the pulse has ended. Scale bars = 30 µm

Supporting Information Figure 5: Cell viability is low at higher voltage amplitudes

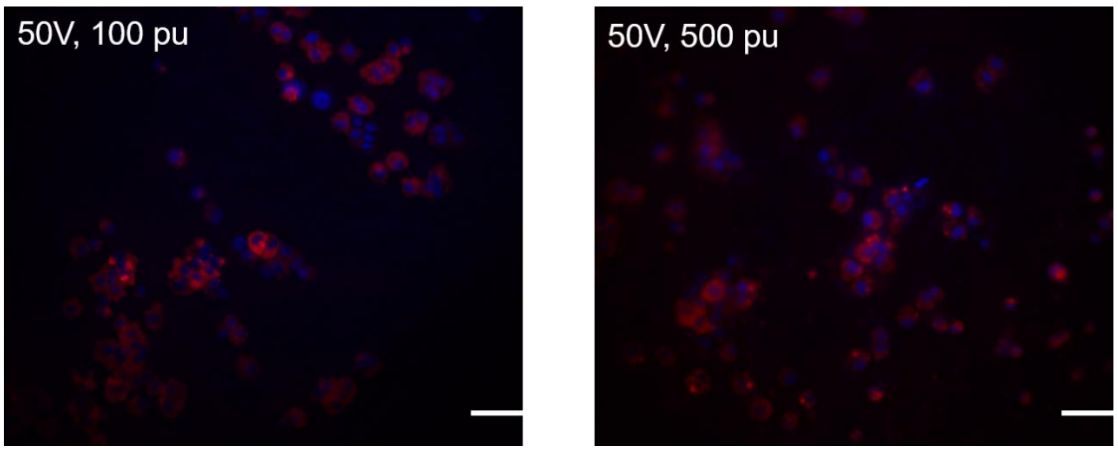

Supporting Information Figure 5: At higher voltage amplitudes (50V for the images shown here), most cells lifted on day 1. Further, the cell morphology looked abnormal. The composite images show tdTomato expression (red) and cell-nuclei (blue). Scale bars = 100 µm.

Supporting Information Figure 6: Model Verification

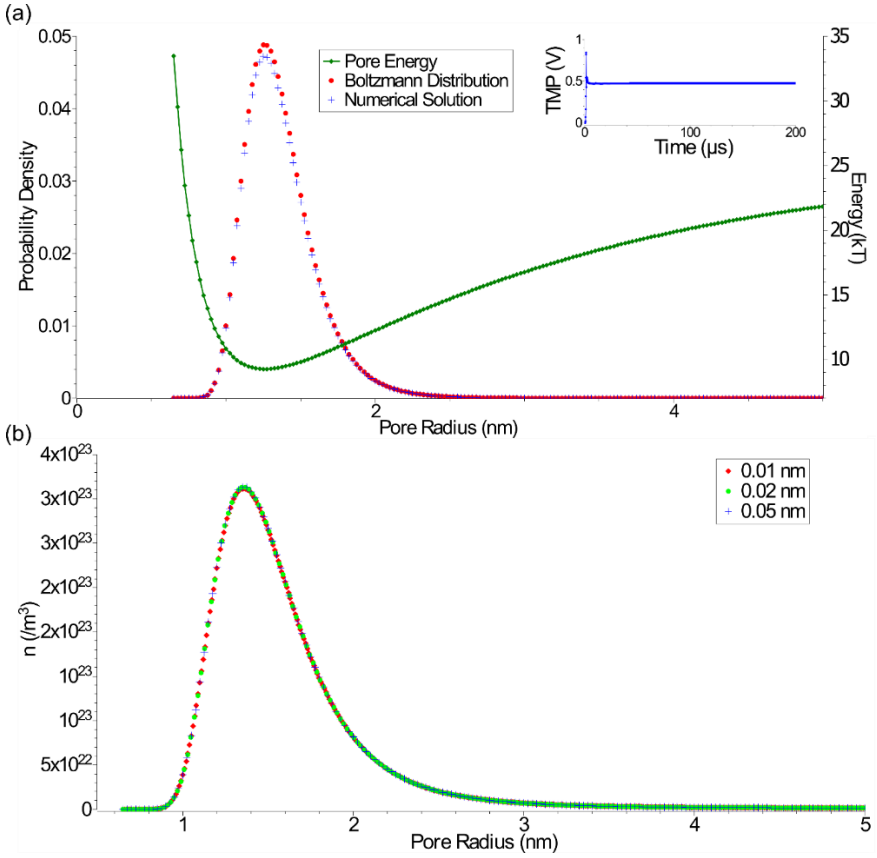

Supporting Information Figure 6: Model Verification (a) The normalized steady state pore distribution ($n/\sum n$) obtained from the numerical simulation (200 μs into the pulse) is plotted as a function of pore radius and compared to the analytical Boltzmann distribution ($e^{-E/kT}/\sum e^{-E/kT}$) where, E is the hydrophilic pore energy (Eq. 2). Inset shows that the TMP has reached a steady state at 200 μs. The steady state solution of the Smoluchowski equation is the Boltzmann distribution, and the analysis serves as a verification for the model, (b) The pore distribution (n) at 50 μs is plotted as a function of pore radius for different mesh sizes. The solution does not change with mesh size. The applied far-field voltage is 15 V for both the cases.

Supporting Information Figure 7: Comparison of LEPD with Lipofectamine Transfection

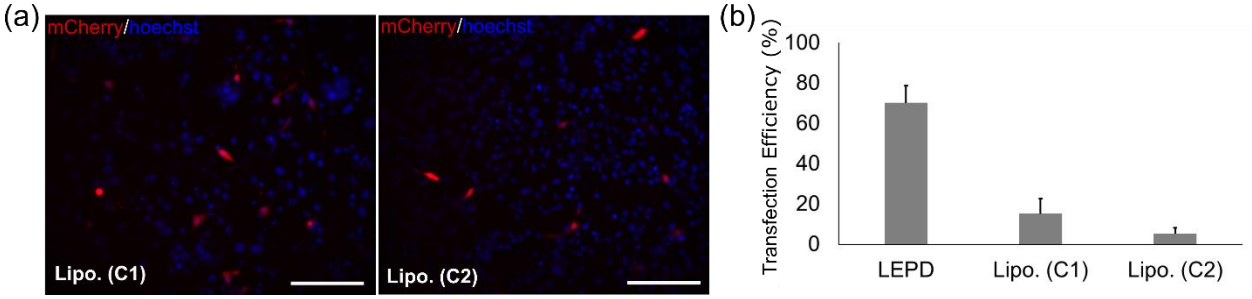

Supporting Information Figure 7: Comparison of LEPD with Lipofectamine Transfection (a) Transfection of mCherry plasmid in MDA-MB 231 cells using lipofectamine under two conditions. Left: Transfection using 0.3 µl of lipofectamine per 100 ng of DNA (C1). Right: Transfection using 0.15 µl of lipofectamine per 100 ng of DNA (C2). Scale Bars = 400 µm, (b) Comparison of transfection efficiencies for the LEPD (using 30 V pulse and hypo-osmolar buffer) and lipofectamine. N=3 for all cases.

References

1. Son, R. S.; Gowrishankar, T. R.; Smith, K. C.; Weaver, J. C. Modeling a Conventional Electroporation Pulse Train: Decreased Pore Number, Cumulative Calcium Transport and an Example of Electrosensitization. *IEEE Trans. Biomed. Eng.* **2016,** *63*, 571-580.
2. Neu, J. C.; Krassowska, W. Asymptotic Model of Electroporation. *Phys. Rev. E* **1999,** *59*, 3471-3482.
3. Pastushenko, V. F.; Chizmadzhev, Y. A.; Arakelyan, V. B. 247 - Electric Breakdown of Bilayer Lipid Membranes II. Calculation of the Membrane Lifetime in the Steady-state Diffusion Approximation. *Bioelectrochem. Bioenerg.* **1979,** *6*, 53-62.
4. Neu, W. K.; Neu, J. C. Theory of Electroporation. In *Card. Bioelectr. Ther.: Mech. Pract. Implic.*; Efimov, I. R.; Kroll, M. W.; Tchou, P. J., Eds.; Springer US: Boston, MA, **2009;** pp 133-161.
5. Neu, J. C.; Smith, K. C.; Krassowska, W. Electrical Energy Required to Form Large Conducting Pores. *Bioelectrochemistry* **2003,** *60*, 107-114.
6. Vasilkoski, Z.; Esser, A. T.; Gowrishankar, T. R.; Weaver, J. C. Membrane Electroporation: The Absolute Rate Equation and Nanosecond Time Scale Pore Creation. *Phys. Rev. E* **2006,** *74*, 021904.
7. Renkin, E. M. Filtration, Diffusion, and Molecular Sieving Through Porous Cellulose Membranes. *J. Gen. Physiol.* **1954,** *38*, 225-243.
8. Bungay, P. M.; Brenner, H. The Motion of a Closely-Fitting Sphere in a Fluid-Filled Tube. *Int. J. Multiphase Flow* **1973,** *1*, 25-56.
9. Parsegian, A. Energy of an Ion Crossing a Low Dielectric Membrane: Solutions to Four Relevant Electrostatic Problems. *Nature* **1969,** *221*, 844.
10. Chernomordik, L. V.; Sukharev, S. I.; Popov, S. V.; Pastushenko, V. F.; Sokirko, A. V.; Abidor, I. G.; Chizmadzhev, Y. A. The Electrical Breakdown of Cell and Lipid Membranes: The Similarity of Phenomenologies. *Biochim. Biophys. Acta, Biomembr.* **1987,** *902*, 360-373.
11. Sten-Knudsen, O. *Biol. Membr.: Theory Transp., Potentials Electr. Impulses*; Cambridge University Press: Cambridge, **2002;** pp 180-190